Coordination Chemistry Reviews, 64 (1985) 93—112
Elsevier Science Publishers B.V., Amsterdam — Printed in The Netherlands

CALCULATION OF EXCITED STATE BONDING CHANGES AND ELECTRONIC SPECTRA FROM PRE-RESONANCE RAMAN SPECTRA

JEFFREY I. ZINK
Department of Chemistry, University of California, Los Angeles, CA 90024 USA

ABSTRACT

Excited state distortions of $W(CO)_5$pyridine, $W(CO)_5$piperidine, $Mo_2(CF_3CO_2)_4$, and $K_3Cr(CN)_5NO$ are calculated from emission spectra and pre-resonance Raman spectra by using the time-dependent theory of molecular spectroscopy. The time-dependent theory is described and the connections between electronic spectra and pre-resonance Raman spectra are discussed. Electronic emission and/or absorption spectra of the above compounds at 10° K are reported. The electronic spectra are calculated from the pre-resonance Raman determined intensities and frequencies. The connections between the excited state bond length distortions and the photochemical reactivity of the molecules is discussed. The "Missing Mode Effect" or MIME effect is explained.

INTRODUCTION

The distortions which a molecule undergoes after it is excited to its excited electronic states are important in determining its spectroscopic and photochemical properties. These excited state distortions can be calculated by using a Franck-Condon analysis when a highly resolved spectrum including vibronic progressions is available (refs.1-8). Unfortunately, the electronic emission and absorption spectra of large organometallic and inorganic molecules in condensed media typically contain broad featureless bands (ref.9). Spectra of these molecules at low temperatures sometimes reveal vibronic structure, but the individual vibronic components are usually not well resolved. Instrumental resolution in these experiments is usually several orders of magnitude greater than the resolution seen in the spectrum.

Detailed calculations of excited state distortions and structures and an intuitive understanding of the meaning of band widths and poorly resolved vibronic features are obtainable from the newly developed time dependent theory of molecular spectroscopy (refs.10-12). The theory connects pre-resonance Raman spectroscopy, electronic absorption and emission spectroscopy, and geometry changes between the ground and excited electronic states. It has recently been applied to a limited number of transition metal and organic systems (refs.13-18).

The purposes of this article are to describe the time dependent theory and to use it to calculate the excited state distortions of large transition metal and organometallic molecules. Pre-resonance Raman spectra and electronic emis-

0010-8545/85/$07.00

sion and/or absorption spectra are reported and analyzed. The intimate connections between these seemingly disparate spectroscopic techniques and between the spectra and the excited state distortions are discussed. The chemical and photochemical importance of the excited state distortions is also discussed.

THEORY

The time-dependent theory of molecular spectroscopy provides both a quantitative and an intuitive physical picture of the inter-relationship between pre-resonance Raman spectra and electronic absorption and emission spectra (refs.10, 11,12). In both types of spectroscopy, the spectra are governed by the motion of a wavepacket on a multidimensional electronic state potential hypersurface. A cross section of the multidimensional surface along one normal mode which will be used to discuss the theory is shown in figure 1.

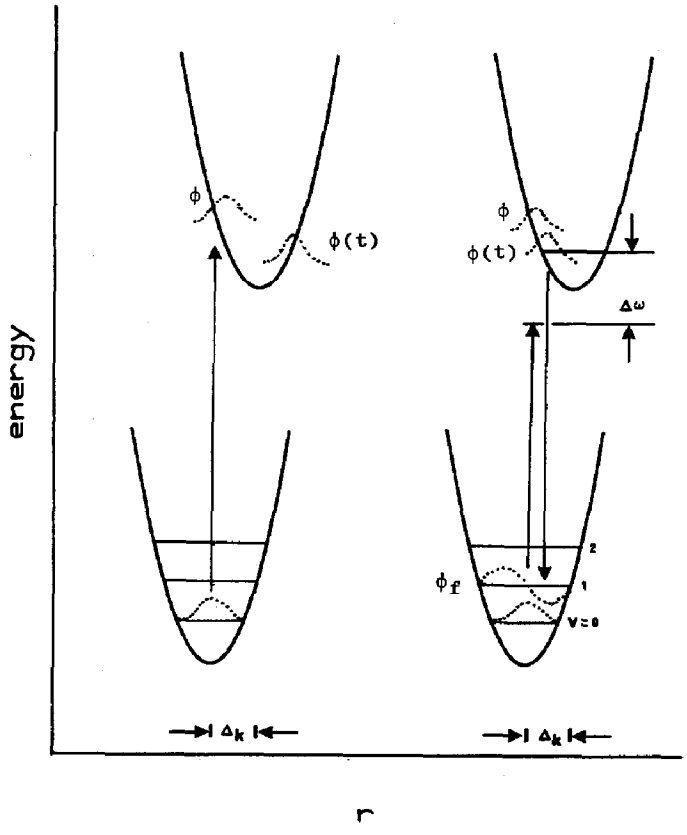

Fig. 1. Illustrations of the time-dependent theory of absorption spectroscopy (left) and of pre-resonance Raman spectroscopy (right).

Electronic Absorption and Emission Spectroscopy

The absorption process is illustrated on the left side of figure 1. The initial vibrational wavepacket, ϕ, propagates on the upper potential surface which, in general, is displaced relative to the ground surface. The displaced wavepacket is not a stationary state and evolves according to the time-dependent Schrodinger equation. The quantity of interest is the overlap of the initial wavepacket with the time-dependent wavepacket, $\langle\phi|\phi(t)\rangle$. The overlap is a maximum at t=0 and decreases as the wavepacket moves away from its initial position. At some later time t, the wavepacket may return to its initial position giving rise to a recurrence of the overlap. A plot of the overlap as a function of time in the time domain shows the initial overlap decreasing and then recurring at a time t when the wavepacket (and thus all of the atoms in the molecule) returns to its original position. This pattern is repetitive. In the simple case of harmonic potential surfaces and no change in vibrational frequencies between the ground and excited electronic states, the overlap is

$$\langle\phi_k|\phi_k(t)\rangle = \exp[-\Sigma_k(\Delta_k/2(1-e^{i\omega_k t} - i\omega_k t/2) - iE_o t/h - \Gamma^2 t^2] \qquad (1)$$

where E_o is the energy difference between the minima of the two surfaces, Γ is a phenomenological damping factor (vide infra), and ω_k and Δ_k are the frequency and the displacement of the k^{th} normal mode.

The electronic absorption spectrum in the frequency domain is the fourier transform of the overlap in the time domain. The absorption spectrum is then given by

$$I(\omega) = C\omega\int_{-\infty}^{\infty} e^{i\omega t} \langle\phi_k|\phi_k(t)\rangle \, dt \qquad (2)$$

where C is a constant, ω is the frequency of incident radiation, and the other quantities are those defined above. Thus, the absorption spectrum can be calculated when the frequencies ω_k and the displacements Δ_k of the normal modes are known.

The time-dependent theoretical treatment of the electronic emission spectrum is very similar to that of the absorption spectrum. The principal difference is that the initial wavepacket starts on the upper (excited state) electronic surface and propagates on the ground electronic state surface. The overlap of the initial wavepacket with the time-dependent wavepacket is given by equation 1. The emission spectrum is given by

$$I(\omega) = C\omega^3\int_{-\infty}^{\infty} e^{i\omega t} \langle\phi_k|\phi_k(t)\rangle \, dt \qquad (3)$$

where all of the symbols are the same as those in eq. 2. Note that for emission, the intensity is proportional to the cube of the frequency times the Fourier transform of the time dependent overlap.

In most transition metal and organometallic compounds, many normal modes are displaced. The expressions discussed above describe the case where one specific normal mode (the k^{th}) is displaced. In the usual case of many displaced normal modes, the total overlap is given by

$$\langle\phi|\phi(t)\rangle = \prod_k \langle\phi_k|\phi_k(t)\rangle \exp(-iE_0 t/h - \Gamma^2 t^2) \qquad (4)$$

where the shift of the electronic energy between the minima of the two surfaces E_0 and a Gaussian damping Γ have been included. The complete overlap is thus

$$\langle\phi|\phi(t)\rangle = \exp\{-\Sigma_k[(\Delta_k^2/2)(1-e^{-i\omega_k t})-i\omega_k t/2]-iE_0 t/h -\Gamma^2 t^2\} \qquad (5)$$

This expression for the complete overlap is Fourier transformed to give the electronic absorption or emission spectrum. In order to carry out the calculation it is necessary to know the frequencies ω_k and the displacements Δ_k for all of the displaced normal modes. In addition, the energy difference between the minima of the two potential surfaces E_0 and the damping Γ must be known. As will be discussed below, the frequencies and displacements can be experimentally determined from pre-resonance Raman spectroscopy, and the energy difference between the ground and excited states and the damping can be obtained from the electronic absorption spectrum and/or emission spectrum.

The damping factor Γ arises because of relaxation into other modes, the "bath", etc. It is instructive to examine the meaning of the damping factor in the time domain. At one extreme, it will have a value of zero if every atom in the molecule returns to exactly its starting position at the same time during the time evolution of the system. This condition means that each of the wavepackets in eq. 4 must have a recurrence in the overlap at time t which is equal to the overlap at t=0. If even one atom of the molecule does not return to exactly its starting position at that time t, the total overlap in eq. 4 will be smaller at time t than at time t=0. The effect of a non-zero damping factor is to decrease the value of the recurrence of the overlaps in the time domain. The effect on the spectrum in the frequency domain is to decrease the resolution, i.e., to "fill in" the spectrum. In the case where the damping is large enough to prevent any recurrence, the spectrum in the frequency domain will consist of only the envelope with no vibronic structure.

Raman Spectroscopy

The time-dependent picture of Raman spectroscopy is shown on the right side

of figure 1. Again the initial wavepacket propagates on the upper excited electronic state potential surface. However, the quantity of interest is the overlap of the time-dependent wavepacket with the final state ϕ_f, i.e. $\langle\phi_f|\phi(t)\rangle$. The Raman scattering amplitude in the frequency domain is the half Fourier transform of the overlap in the frequency domain,

$$\alpha_{fi}(\omega_I) = \int_0^\infty e^{i\omega_I t - \Gamma t} \langle\phi_f|\phi_i(t)\rangle \, dt \tag{6}$$

It is very difficult to experimentally obtain the values of the scattering cross section. However, it is relatively easy to obtain the intensity of given normal mode k relative to that of another mode k'. A simple expression relating the relative intensities has been derived for the special conditions of harmonic oscillators, no Duschinsky rotation, no change in normal mode frequencies, and pre-resonance (short time) condition spectra. Under these conditions the relative intensities of two modes is given by

$$\frac{I_k}{I_{k'}} = \frac{\Delta_k^2 \omega_k^2}{\Delta_{k'}^2 \omega_{k'}^2} \tag{7}$$

The important experimental condition which must be fulfilled is the short time, pre-resonance condition. When the incident frequency is slightly off resonance with the excited electronic state of interest, the propagation time of the wavepacket on the upper potential surface is governed by the time-energy uncertainty principle $\Delta\omega\Delta t \tilde{>} 1$ where $\Delta\omega$ is the frequency mismatch. Under short time conditions the wavepacket moves in a region localized near the equilibrium geometry of the ground electronic state, i.e., the Franck-Condon region. The pre-resonance Raman intensity is dominated by the slope of the potential surface in this region. The greater the slope, the greater the motion of the wavepacket in figure 1, the greater the overlap with the final state and the greater the intensity.

Calculation of Excited State Distortions and Electronic Spectra from Raman Intensities

The dynamics of the wavepacket on the upper potential surface determines both the absorption spectrum and the Raman spectrum. (The emission spectrum is determined by the dynamics on the ground state potential surface with the same displacements as those which determine the absorption and Raman.) In the short time limit, the intensities in the Raman spectrum are related to the displacements by eq. 7. In the short time limit, the absorption spectrum becomes

$$I(\omega) = C\omega \exp[-(\omega-E)^2/2\sigma^2] \tag{8}$$

The quantity $2\sigma^2$ is the width of the electronic absorption spectrum at 1/e of the height. This quantity is also related to the displacements

$$2\sigma^2 = \sum_k \Delta_k^2 \omega_k^2 \qquad (9)$$

Thus $2\sigma^2$ is experimentally found from the absorption spectrum, ratios of the Δ's are found from the Raman spectrum, and the Δ_k's are calculated (except for sign) by pairwise comparison of the Raman intensities. Once the Δ_k's are calculated, the electronic spectra are calculated by using eq. 2 or 3.

APPLICATIONS

Three applications of the theoretical and spectroscopic techniques are discussed below. First, the techniques are applied to $W(CO)_5$pyridine and $W(CO)_5$piperidine. The connections between the excited state distortions and the photochemical reactions are described. A new spectroscopic effect, the MIME effect, is defined and discussed. Second, the techniques are applied to a metal-metal quadruple bond (fig.2). Bond length changes between the metals as well as between the metal and the ligands are determined. Third, a brief example of an extension of the techniques to the analysis of distortions using overtone intensities is presented.

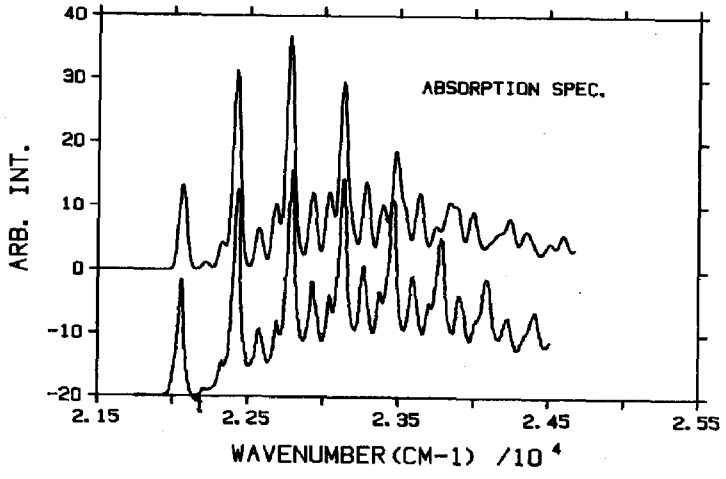

Fig.2. Absorption spectra of $Mo_2(CF_3CO_2)_4$. These spectra show much higher resolution than is usually observed. Spectra of the type in the next three figures are much more common. The experimental (bottom) and calculated (top) spectra shown here are discussed later in the text.

$W(CO)_5$pyridine and $W(CO)_5$piperidine

The application of the time-dependent theory to these substituted tungsten carbonyl compounds is a prototypical case study of the use and the power of the techniques. Emission spectroscopy, pre-resonance Raman spectroscopy and the time-dependent theory are used.

Spectroscopy. The emission spectrum of a single crystal of $W(CO)_5$py taken at 10°K is shown in fig. 3. The emission has been assigned to the $^3E \rightarrow {}^1A_1$, d_z2 to (d_{xz},d_{yz}) transition (refs.19-23). The spectrum shows two types of resolved structure: a low frequency progression with a peak to peak separation of 90 cm^{-1}, and a long regularly spaced progression with a peak to peak separation of 550±10 cm^{-1}. The emission spectrum of $W(CO)_5$py in a 2-MeTHF glass at 10°K showed the 550 cm^{-1} progression but did not contain the 90 cm^{-1} peaks. Thus the 90 cm^{-1} peaks are tentatively assigned to a crystal lattice mode. The most unusual aspect of the spectra is the 550 cm^{-1} progression. In a luminescence spectrum, a regularly spaced progression is almost always caused by distortion

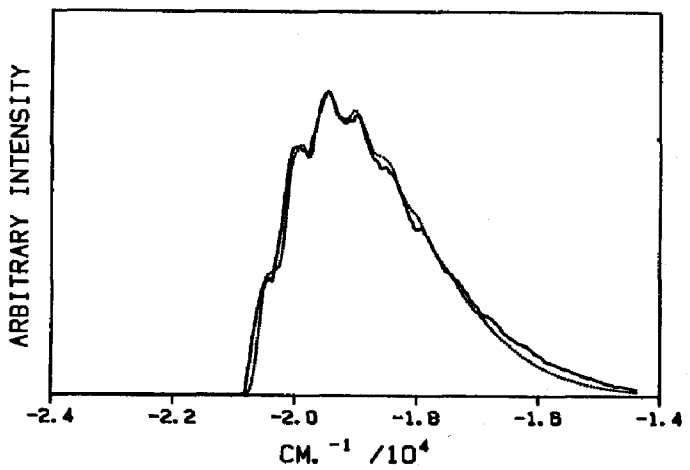

Fig.3. Experimental (solid line) and calculated (dotted line) emission spectra of $W(CO)_5$pyridine. The calculated spectrum was obtained by using exactly the preresonance Raman determined distortions given in table 1.

along a totally symmetric normal mode whose frequency is equal to the vibrational frequency of that mode in the ground electronic state. Surprisingly, there are no totally symmetric normal modes with a frequency of 550 cm^{-1} (vide infra).

The emission spectrum of a single crystal of $W(CO)_5$piperidine is shown in fig 4. The emission is assigned to the $^3E \rightarrow {}^1A_1$, d_z2 to (d_{xz},d_{yz}) transition. Two progressions are again observed. The smaller progression with a peak to peak separation of 80 cm^{-1} is again attributed to a crystal lattice mode for the same reasons as above. The second progression is a long, regularly spaced progression with a peak separation of 520 ± 15 cm^{-1}. The major difference between this spectrum and that of the pyridine complex is that the progression is significantly longer. The peak maximum occurs at the sixth vibrational quantum instead of the third. This progression is also unusual because there is no ground state normal vibrational mode with an energy near 520 cm^{-1} (vide infra).

The pre-resonance Raman data for $W(CO)_5$py and $W(CO)_5$piperidine are given in table 1. The relative intensities of the peaks were determined by integrating the peaks. All of the peaks in the experimental spectrum having intensities

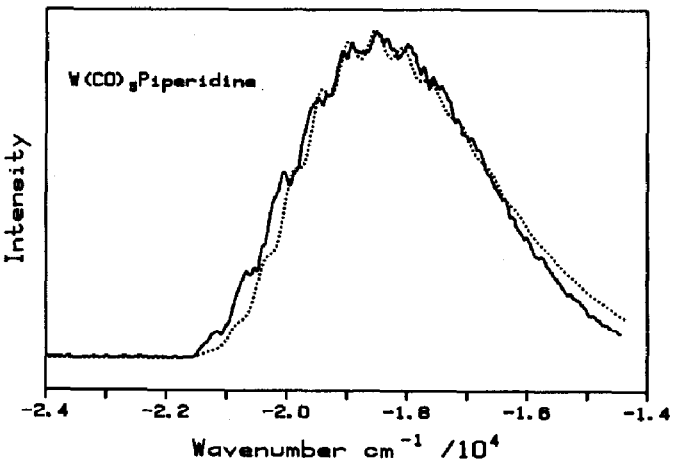

Fig.4. Experimental (solid line) and calculated (dotted line) emission spectra of $W(CO)_5$piperidine. The calculated spectrum was obtained by using the preresonance Raman determined distortions given in table 1.

TABLE 1

Preresonance Raman Intensities and Calculated Distortions.

	$W(CO)_5$pyridine		
$\omega_k(cm^{-1})$	I_k/I_{636}[a]	Δ_k/Δ_{636}[a]	emission best fit
2075	1.82(0.51)	0.28(0.04)	0.28
1973	1.27(0.36)	0.24(0.03)	0.24
1953	0.46(0.13)	0.15(0.02)	0.15
1934	0.38(0.11)	0.14(0.02)	0.14
1890	1.36(0.38)	0.27(0.04)	0.27
1651	0.47(0.13)	0.18(0.03)	0.18
1607	2.18(0.61)	0.39(0.05)	0.39
1489	0.10(0.03)	0.10(0.01)	0.10
1223	1.45(0.41)	0.43(0.06)	0.43
1073	0.83(0.23)	0.37(0.05)	0.37
1012	3.59(1.01)	0.81(0.11)	0.81
636	1.00(0.28)	0.68(0.10)	0.68
602	0.79(0.22)	0.64(0.09)	0.64
470	0.38(0.11)	0.56(0.08)	0.56
462	0.86(0.24)	0.87(0.12)	0.87
434	1.17(0.32)	1.08(0.15)	1.08
427	1.00(0.28)	1.01(0.14)	1.01
195	0.41(0.12)	1.42(0.20)	1.42
	$W(CO)_5$piperidine		
$\omega_k(cm^{-1})$	I_k/I_{484}[b]	Δ_k/Δ_{484}	emission best fit
2950	0.21	0.13	0.14
2930	0.26	0.14	0.16
2069	0.94	0.39	0.43
1982	0.56	0.32	0.36
1970	1.71	0.56	0.61
1919	0.35	0.27	0.31
1905	0.40	0.29	0.32
1860	1.09	0.49	0.54
1837	0.83	0.43	0.49
1030	0.05	0.20	0.22
810	0.10	0.34	0.38
596	0.14	0.54	0.79
484	1.00	1.78	2.38
433	0.82	1.80	1.80
426	0.60	1.57	1.54
414	0.90	1.96	1.58
377	0.05	0.49	0.54
256	0.08	0.93	0.85

a. Experimental uncertainties are given in parentheses.
b. Experimental uncertainties are ±15%.

greater than three percent of that of the most intense peak were measured and used in the calculations.

The electronic spectrum is calculated by using equations 3 and 5. The distortions used in these equations are determined from the pre-resonance Raman intensities by using equations 7 and 9. Both the vibrational frequencies of the normal modes and the displacements of the excited state potential surfaces along these normal modes are obtained from the pre-resonance Raman spectrum. The intensity of a Raman peak at a given frequency is related to the slope of the excited state potential surface along that normal mode. The greater the slope, the greater the displacement, the greater the motion of the wavepacket, the greater the overlap, and thus the greater the Raman intensity.

Once the displacements of the excited state surface along the normal modes are determined, the wavepacket is propagated on the multidimensional hypersurface and the overlap $\langle\phi|\phi(t)\rangle$ is calculated from equation 5. The overlap in the time domain is then Fourier transformed (eq. 3) to give the calculated electronic spectrum. When good agreement with experiment is found, the agreement indicates that the simplifying assumptions discussed previously are met and that the distortions which are calculated are meaningful.

The emission spectrum of $W(CO)_5py$ calculated as discussed above is shown in fig. 3. In this calculation exactly the displacements and frequencies described from the experimental Raman data given in table 1 were used. Excellent agreement between the experimental spectrum and the theoretical spectrum calculated from the 18 dimensional excited state potential surface is obtained. Interpretation of these results will be discussed below.

The calculated emission spectrum of $W(CO)_5pip$ is shown superimposed on the experimentally determined spectrum in figure 4. The agreement between the calculated and experimental spectra is not as good as that in figure 3. Two factors are probably involved. First, the excited state is significantly more distorted than that in $W(CO)_5py$. Thus more vibrational quanta are involved and anharmonicity, which was not included in the calculation, will play a larger role. Secondly, the W-N stretching mode was not observed in the Raman spectrum. It is probably at lower energy than the W-N stretch in the pyridine complex. Even if a low frequency mode has a significant distortion, the observed relative intensity will be small because of the inverse frequency squared term in eq. 7. The major effect of a very low frequency mode on the emission spectrum can be included in the damping factor (vide infra). These considerations explain why a larger damping factor is required for piperidine than for pyridine.

The excited state geometries of the $W(CO)_5py$ and $W(CO)_5pip$ complexes in their lowest excited electronic states are calculated by converting the relative displacements, given in table 1, to bond length changes in A units. First, the relative displacements are converted to absolute displacements by using eqs. 7

and 9. The value of $2\sigma^2$ is obtained from the absorption spectrum. The resulting displacements, Δ_k, are converted from dimensionless normal coordinates to lengths and angles by transforming to the desired units. A complete calculation requires a complete normal coordinate analysis. A good approximation is achieved by assuming that the normal coordinates are uncoupled and that the masses appropriate to a specific normal coordinate can be used. The latter calculation is reported here because a complete normal coordinate analysis is not available for the molecules studied in this paper.

The calculated changes in the bond lengths (in A) for $W(CO)_5py$ show that the most highly elongated bond is the W-N bond. The W-C bond trans to the pyridine is also highly elongated. The lengths of the W-C bonds cis to the pyridine are only slightly changed. The excited state bond length changes are W-N, 0.18 Å, trans W-C, 0.12 Å, and cis W-C, 0.04 Å. All of the WCO bond angles of the carbonyls cis to the pyridine are changed from 180°. A determination of the angle change in degrees requires a normal coordinate analysis. The meaning of the bond length changes in terms of the bonding changes in the excited state and the connections of these bond lengthenings to the photochemical reactivity of the molecule are discussed below.

The bond length changes in the $W(CO)_5pip$ complex are larger than those in the pyridine complex. The W-C bond trans to the piperidine is lengthened by 0.25 Å and the cis W-C bonds are lengthened by 0.05 Å. The bond length change of the W-N bond has an upper limit of 0.3 Å.

Orbital Characteristics of the Lowest Excited State. The lowest energy excited state of $C_{4v}W(CO)_5L$ compounds, (where L is a ligand lower in ligand field strength than CO), has been assigned by Wrighton, et al., to the (d_{xz}, d_{yz}) to d_z2 transition (refs.19,20). This assignment has been confirmed by detailed spectroscopic studies including MCD spectroscopy (refs.24,26). Both the pyridine and piperidine complexes have ^3E lowest energy excited states.

The orbital components of the lowest energy excited state in C_{4v} d^6 complexes are given by equation 10 (ref.27). Because of the proximity of other states of the same symmetry, mixing occurs and some $d_{x^2-y^2}$ orbital character is involved.

$$\phi_E = \frac{1}{\sqrt{1+\lambda^2}}\left[\frac{\sqrt{3}+\lambda}{2}\,(d_{xy}{}^2 d_{xz}{}^2 d_{yz}{}^1 d_{z^2}{}^1) + \frac{1-\sqrt{3}\lambda}{2}\,(d_{xy}{}^2 d_{xz}{}^2 d_{yz}{}^1 d_{x^2-y^2}{}^1)\right] \qquad (10)$$

The mixing coefficient λ is related to the difference between the ligand field strengths of the carbonyl ligand and the unique ligand (ref.27). For an octahedron (where L=CO), $\lambda = 0$ and the sigma interactions between the metal and all six ligands are equal. When the unique ligand L is weaker than carbonyl as is the case for pyridine and piperidine, $\lambda < 0$ and the increase in d_z2 character over $d_{x^2-y^2}$ character causes increased sigma antibonding in the z direction

compared to that in the xy plane. The relationship between λ and the percent d_z^2 character has been discussed in detail. The most important conclusions from these orbital considerations are 1) that in the one-electron ligand field orbital picture of $W(CO)_5$py and $W(CO)_5$pip, the d_z^2 orbital lies lower in energy than the $d_{x^2-y^2}$ orbital and 2) that the lowest energy excited state wavefunction is dominated by a large d_z^2 character.

The excited state distortions can be predicted from the orbital characteristics (ref.28). The d_z^2 orbital and the $d_{x^2-y^2}$ orbital are both sigma antibonding molecular orbitals. Populating the d_z^2 orbital is thus expected to weaken sigma bonding primarily in the z direction. Populating the $d_{x^2-y^2}$ orbital is expected to weaken sigma bonding in the xy plane. The larger the value of λ in equation 10, the greater the bond weakening in the z direction (ref.28).

The largest distortion expected for $W(CO)_5$py and $W(CO)_5$pip, based on the above considerations, is metal-ligand bond lengthening along the z axis, the axis containing the unique ligand. Smaller but non-zero distortions are also to be expected in the xy plane. Although metal-ligand bond lengthenings are predicted to be the biggest distortions, small changes in bond lengths in the ligands themselves are also expected. For example, lengthening a W-CO bond should reduce back bonding to the CO thus strengthening the CO bond and decreasing the CO bond length. Small changes are also expected in the pyridine ring.

Trends in the magnitudes of the major distortions can also be predicted from equation 10. The piperidine ligand is a weaker ligand in the spectrochemical series than pyridine. (The energy of the absorption maximum is 22,100 cm^{-1} in $W(CO)_5$pip and 22,400 cm^{-1} in $W(CO)_5$py.) Thus λ is larger for the piperidine complex than that for the pyridine complex and the distortions along the z axis should be greater.

The experimental results provide the first spectroscopic substantiation of the ligand field based bonding predictions. The largest experimentally determined distortions occur along the z axis and smaller distortions occur along in the xy plane. The piperidine complex is more highly distorted than the pyridine complex. Small distortions of the bond lengths within the ligands are also observed. The predicted bonding changes which have been used to predict photochemical reactivity are verified by the combination of pre-resonance Raman spectroscopy, electronic spectroscopy, and time-dependent theory.

Correlations between Excited State Distortions and Photochemical Reactivity. The ligand field theory of transition metal photochemistry is based on the idea that the bonding changes in excited electronic states are correlated with ligand photolabilization (refs.29-31). Populating the d_z^2 or $d_{x^2-y^2}$ orbitals increases sigma antibonding in the z and xy directions respectively. Depopulating d orbitals which have pi symmetry simultaneously change the pi bond order with a directionality determined by which d orbital is depopulated. Sigma and

pi bond weakening along a given metal-ligand bond is correlated with the photochemical ligand labilization of that bond.

In cases such as those studied here where two different ligands are on the same molecular axis such as the z axis, the more complicated question of which of the two ligands experiences the greatest antibonding arises. Three approaches to answering this question have been used. The first successful approach used molecular orbital theory, specifically overlap populations, to calculate the distribution of antibonding along a given axis (ref.32). This approach is predictive, but it requires a complete calculation for each compound of interest. A second approach uses ligand field theory. When the original theory is rewritten in terms of angular overlap parameters, contributions from each ligand can be apportioned (ref.31). This approach is also predictive, but is not useful for many metals because the required parameters have not or cannot be determined. The third approach, used specifically for tungsten carbonyls, is an empirical analysis based on infrared data (ref.21). It is to some extent predictive for compounds far from the empirical dividing lines. The above three approaches are indirect methods of inferring antibonding character in a given excited state.

The bond length changes determined from pre-resonance Raman spectra, electronic spectra and time dependent theory provide a detailed picture of the results of bonding changes caused by populating excited electronic states. There is a direct but not linear correlation between bond length changes and the photochemical labilizations of the ligands. In the pyridine complex, the most highly distorted metal-ligand bond, the W-N bond, is lengthened by 0.20 A. The quantum yield for pyridine loss is 0.2. The much less distorted metal-carbon bond is much less reactive; the quantum yield for CO loss is less than 10^{-2}. It is interesting to note that the piperidine complex has a larger distortion and a larger quantum yield for reaction than the pyridine complex. Further work is needed to determine whether or not such a correlation is general for $W(CO)_5L$ complexes.

The Missing Mode Effect (MIME) Both of the compounds $W(CO)_5py$ and $W(CO)_5pip$ exhibit the "Missing Mode Effect" (MIME), a regularly spaced vibronic progression in the luminescence spectrum which does not correspond to any ground state normal mode vibration. In the luminescence spectrum of $W(CO)_5py$, the MIME spacing is 550 cm^{-1}, and in the luminescence spectrum of $W(CO)_5pip$ the MIME spacing is 520 cm^{-1}. No totally symmetric vibrational modes of these frequencies are found in the vibrational spectra of these molecules (refs.33,34).

The MIME effect is easily understood from the viewpoint of time dependent theory. In the time domain, the most important characteristics of the overlap are the rapid falloff near t=0, the partial recurrence in the overlap near $t_m=2\pi/w_m$ (where w_m is the frequency spacing of the observed progression in the

frequency domain), and the quenching of further recurrences in the time domain due to the damping factor Γ and to the presence of displacements in several different modes. The partial recurrence at $t=t_m$ is responsible for the appearance of the regularly spaced progression at frequency $w_m=2\pi/t_m$. Two or more displaced modes can conspire to give such a partial recurrence which is not expected of any mode alone. In the simplest pedagogical example, a two mode case, the total overlap is

$$\langle\phi|\phi(t)\rangle = \langle\phi_1|\phi_1(t)\rangle\langle\phi_2|\phi_2(t)\rangle \exp(-iE_o t/h-\Gamma^2t^2) \qquad (11)$$

If $\langle\phi_1|\phi_1(t)\rangle$ and $\langle\phi_2|\phi_2(t)\rangle$ peak at different times, the product $\langle\phi|\phi(t)\rangle$ may peak at some intermediate time. The compromise recurrence time t_m is not just the average of t_1 and t_2. The MIME frequency may be smaller than any of the individual frequencies, but it is usually between the highest and lowest frequencies. It cannot be larger than the highest frequency.

Each of the displaced modes in the molecule can contribute to the MIME frequency. Each of these modes k has a time dependence whose magnitude is given by eq. 1 . The larger the displacement Δ_k in the k^{th} mode, the sharper the peaks in $\langle\phi_k|\phi_k(t)\rangle$. The total overlap $\langle\phi|\phi(t)\rangle$ is the product (eq. 10) of the individual modes' overlaps and t_m will tend to be closest to $t_k=2\pi/w_k$ for that mode with the largest Δ_k.

The 550 cm^{-1} MIME frequency of $W(CO)_5py$ was calculated by using the Raman-determined distortions and frequencies as described in the theory and results sections above. The normal modes which give a recurrence in the time domain at $t=t_m$ (i.e., a MIME frequency $w_m=2\pi/t_m=550$ cm^{-1}) are predominantly the W-C stretches in the 400-500 cm^{-1} region, the WCO bend at 636 cm^{-1} and the W-N stretch at 195 cm^{-1}. Although all of the modes including the high frequency CO stretching modes contribute to the MIME frequency, the primary effect on the luminescence spectrum of these modes with small displacements is to "fill in" the red end of the spectrum.

The 520 cm^{-1} MIME frequency of $W(CO)_5pip$ was calculated by using the same procedures as those used for $W(CO)_5py$. The major contributing modes to the MIME frequency are the W-C stretches in the 400-500 cm^{-1} region and the WCO bending mode at 596 cm^{-1}.

The emission spectra of $W(CO)_5py$ and $W(CO)_5pip$ are typical of the spectra obtained from perturbed polyatomic molecules. The spectra show structure on a scale of five hundred wavenumbers although the instrumental resolution is two orders of magnitude higher. The natural tendency to interpret the regularly spaced progression in terms of one displaced mode is far from correct. Instead, eighteen displaced modes contribute to the deserved MIME progression. The origin of the MIME effect is readily explained by using time-dependent theory. In

addition, displacements of the modes, (which are hidden in the emission spectrum) are determined.

Dimolybdenum Compounds. Bond Length Changes in the $\delta \rightarrow \pi^*$ Excited State.

Excited state distortions can provide important chemical insight into the electronic structure of metal compounds. The electronic spectra and structure of binuclear molybdenum complexes containing formal quadruple bonds are attracting increasing interest (refs.35-42). A highly resolved vibrational structure has been reported on the 23,000 cm^{-1} $\delta \rightarrow \pi^*$ transition in tetrakis(μ-trifluoroacetato)dimolybdenum (III) (ref.39). An interesting question about this transition is how big a change in the metal-metal bond is caused by depopulating the δ orbital and populating the π^*orbital. In addition, it is important to know which other bonds in the molecule are affected by the transition. The techniques discussed above provide an experimental answer to these questions. In this section, we apply pre-resonance Raman spectroscopy, absorption spectroscopy, and time-dependent theory to determine the bond length changes. The excited state distortions of 13 normal modes are determined. The elongation of the Mo-Mo bond is smaller than expected and significant distortions are found in the metal-ligand bonds.

The excited-state distortions of the 14 most highly distorted normal modes were calculated from eq 7 and are given in Table 2. The calculated spectrum is

TABLE 2

Distortions and Intensities from the Raman Spectrum and Theoretical Values Used To Calculate the Electronic Absorption Spectrum

freq. cm^{-1}	Raman values		abs spectrum
	I_k/I_{Mo-Mo}[a]	Δ_k/Δ_{Mo-Mo}	Δ_k/Δ_{Mo-Mo}[b,c]
263	0.10 ± 0.02	0.43 ± 0.04	0.42
395	1.00 ± 0.00	1.00 ± 0.00	1.00
502	0.84 ± 0.31	0.65 ± 0.11	0.30
515	1.02 ± 0.31	0.69 ± 0.10	0.34
774	0.31 ± 0.08	0.25 ± 0.04	0.21
875	0.14 ± 0.05	0.15 ± 0.03	0.14
1184	0.13 ± 0.03	0.11 ± 0.01	0.09
1212	0.17 ± 0.04	0.12 ± 0.01	0.10
1245	0.16 ± 0.04	0.11 ± 0.02	0.10
1463	2.98 ± 0.69	0.42 ± 0.05	0.28
1486	1.82 ± 0.40	0.32 ± 0.04	0.25
1560	0.15 ± 0.03	0.09 ± 0.01	0.09
1592	0.20 ± 0.05	0.10 ± 0.05	0.10

[a]Calculated by integrating the Raman peaks.
[b]ν(Mo-Mo) in the excited state is 355 cm^{-1}. All other frequencies used in the calculation are the Raman-determined values.
[c]The values used in eq 1 were Γ= 20 cm^{-1} and E_0=22064 cm^{-1}, total scaling of distortion is 2.15.

compared to the published spectrum in Figure 2.

Three aspects of the figure should be noted. First, the electronic spectrum calculated from the Raman data is in excellent agreement with the experimental spectrum through five quanta of vibrational excitation. The fit in the high-energy region is not as good because of anharmonicity which was not included in the calculation, and/or the presence of a second electronic transition in this region. Second, the displacements that give the best fit to the absorption spectrum are equal to those determined from the Raman spectrum within the experimental uncertainty of the Raman intensity measurements (± 20%). Finally, the small peak at 22217 cm^{-1} cannot be fit by using the Raman data, supporting the interpretation that it arises from a different electronic state (refs.36, 39).

The consistency between the absorption and Raman data provides a new picture of the excited-state distortions. The elongation of the Mo-Mo bond in the excited state is only 0.045A, much smaller than 0.1 A value, which is obtained on the assumption that only one normal mode is distorted (ref.39). Instead, the entire Mo-O-C-O-Mo ring is enlarged. Populating the π^* orbital has only a small effect on the Mo-Mo bond length.

Distortions in $K_3Cr(CN)_5NO$ from Overtone Intensities.

In the studies of the $W(CO)_5L$ compounds and the metal-metal bond discussed above, the multimode displacements were calculated by using the intensities of fundamentals in Raman spectra. In principle, resonance Raman overtone intensities can provide complimentary information, but in practice they rarely exhibit significant intensity in polyatomic molecules with many displaced normal modes (ref.12).

The $Cr(CN)_5NO^{3-}$ ion possesses almost ideal spectroscopic characteristics for determining excited state distortions from Raman overtone intensities. There are a relatively small number of significantly displaced normal modes, thus giving both a relatively large overtone intensity (18% of that of the fundamental) and concomitantly enough fundamentals to provide a cross check of the calculation. In addition, the electronic absorption spectrum exhibits enough vibronic structure at low temperature (ref.43) to enable the E_{oo} band to be observed and thus allow accurate tuning of the laser to exact resonance with the electronic origin. The successful calculation of the absorption spectrum from the Raman-determined displacements provides a second cross check. The results discussed below represent the first calculation of the displacement of a potential surface along a given normal mode in a multi-mode, polyatomic transition metal complex from the intensity of its overtone.

The displacement Δ_k of the excited state potential surface along the k^{th} normal mode of frequency ω_k is given by (ref.12)

$$\Delta_k^2 = \frac{I_{20}^k}{I_{10}^k} \frac{4\sigma^2}{\omega_k^2} \frac{\varepsilon_1\left(\frac{W_I - E}{\sigma}\right)}{\varepsilon_2\left(\frac{W_I - E}{\sigma}\right)} \qquad (12)$$

I_{20}/I_{10} is the intensity ratio of the overtone to the fundamental, σ^2 is related to the absorption band width, and ε_n is a function based on the energy difference between the absorption band maximum and the laser Raman excitation (ref.10).

The resonance Raman and electronic absorption spectra are shown in figure 5. By using the 1st overtone intensity (table 3), the absorption spectral line

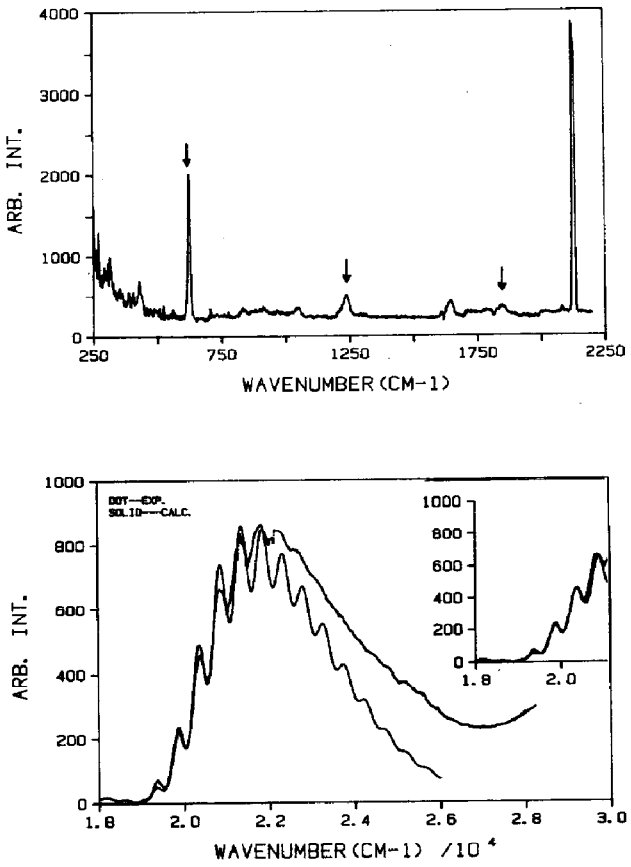

Fig.5. Top: Raman spectrum of $K_3Cr(CN)_5NO$ excited at 514.5 nm. The arrows indicate the fundamental and first and second overtones of the Cr-N stretching mode. Bottom: Experimental (dots) and calculated (solid) electronic absorption spectra. Note the presence of a shoulder at 25000 cm^{-1} and the tail of the next peak at 28000 cm^{-1}. The spectrum was calculated using Γ = 93 and the following frequencies and displacements: 400 cm^{-1}, 1.60; 530 cm^{-1}, 260; 1500 cm^{-1}, 0.26; and 1900 cm^{-1}, 0.80. The insert shows the region near the origin and the spectrum calculated using exactly the Raman-determined displacements, Γ = 105, and frequencies of 400 cm^{-1}, 530 cm^{-1}, 1645 cm^{-1}, and 2128 cm^{-1}.

width and an $\varepsilon_1/\varepsilon_2$ ratio of 0.752, the displacement along the Cr-N stretching normal mode calculated using eq. 1 is 2.20. (Assuming that this coordinate is purely the uncoupled M-N stretch, this displacement is 0.09A.) As a check, the displacement along this normal coordinate is calculated from the intensities of the fundamentals using methods previously described. The displacement calculated using these complementary methods is 2.60 (±0.10A). The two calculated displacements agree within experimental error.

The value of the Raman methods for determining the displacement is especially apparent because the usual Franck-Condon calculation is not feasible. The electronic absorption band (assigned by Gray, et al. to the $^2B_2 \rightarrow {}^2B_2$, metal to NO charge transfer)(ref.43) exhibits resolved vibronic structure. However, the spacing between the vibronic features is not regular. Furthermore, the band is overlapped by additional bands on its high energy side which are revealed by polarization studies. The low energy features of the electronic spectrum which are unencumbered by the overlapping bands can be calculated from the Raman-determined displacements. The calculation uses time-dependent theory and the multi-dimensional excited state surface obtained from the Raman-determined displacements. An excellent fit to the low energy features was achieved using exactly the displacements determined from the Raman intensities for the four normal modes. The vibronic features are thus a result of all of the displaced normal modes (i.e., a type of MIME (ref.16)) and not the result of a single mode. The calculated electronic spectra provide a further check and verify the accuracy of the Raman-determined displacements.

These results show that overtone intensities can be reliably used to calcu-

TABLE 3

Raman Intensities and Calculated Distortions

$\omega_k(cm^{-1})$	assignment	I_k/I_{624} [b]	Δ_k [c]	Δ_k [d]
428	Cr-C [a]	0.13 ± 0.03	1.37 ± 0.30	0.07
624	Cr-N [a]	1.00 ± 0.20	2.60 ± 0.50	0.10
1645	NO [a]	0.07 ± 0.01	0.26 ± 0.05	0.01
2128	CN [a]	1.42 ± 0.28	0.90 ± 0.20	0.03
1237	1st overtone	0.18 ± 0.04	2.20 ± 0.40	0.09
1848	2nd overtone	0.09 ± 0.02	N/A	N/A

a. Assignment from ref. 43
b. Integrated intensity ratios using 514.5 nm excitation. The intensity ratio of the overtone to fundamental is 0.30 when excited at 488 nm. The calculated displacement is 2.0 ± 0.4. The overtone was too weak to be observed under 632.8 nm and 647.1 nm excitation.
c. Dimensionless normal coordinates.
d. Displacements in A assuming uncoupled normal modes. More accurate values require a normal coordinate analysis.

late excited state displacements. These data also shed light on the underlying mechanism giving rise to the overtone intensity. Of the two possible limiting mechanisms derived from time dependent theory, displaced excited states or vibrational frequency changes in excited states (ref.10), the former is over two orders of magnitude more important than the latter for $Cr(CN)_5NO^{3-}$. Ziegler and Albrecht have discussed seven origins of overtone intensity and have shown that the displaced excited state mechanism is expected to become important as resonance is approached (ref.44). The calculation of excited state displacements from overtone intensities is a new tool in the study of the electronic structure of metal complexes.

Acknowledgments.

I thank my co-workers Lee Tutt, Y. Yang, J. Schindler, D. Tannor and C. Yoo for their many contributions to this work. Helpful discussions with Prof. E. Heller are gratefully acknowledged. The U.S. Army Research Office and the National Science Foundation provided the financial support.

REFERENCES

1 H. Yersin, H. Otto, J.I. Zink and G. Gliemann, J. Am. Chem. Soc., 102 (1980) 951, and references therein.
2 H.H. Patterson, J.J. Godfrey and S.M. Kahn, Inorg. Chem., 11 (1972) 2872.
3 H.H. Patterson, W.J. DeBerry, J.E. Byrne, M.T. Hsu and J.A. LoMenzo, Inorg. Chem.
4 K.W. Hipps, G.A. Merrell and G.A. Crosby, J. Phys. Chem. 80 (1976) 2232.
5 R.B. Wilson and E.I. Solomon, Inorg. Chem. 17 (1978) 1729.
6 R.B. Wilson and E.I. Solomon, J. Amer. Chem. Soc., 102 (1980) 4085.
7 S.F. Rice, R.B. Wilson and E.I. Solomon, Inorg. Chem., 19 (1980) 3425.
8 G. Eyring and H.H. Schmidtke, Ber. Bunsenges Phys. Chem., 85 (1981) 597.
9 G.L. Geoffroy and M.S. Wrighton, Organometallic Photochemistry, Academic Press, New York, 1979.
10 E.J. Heller, J. Chem. Phys. 62 (1975) 1544.
11 E.J. Heller, Acc. Chem. Res. 14 (1981) 368.
12 E.J. Heller, R.L. Sundberg and D. Tannor, J. Phys. Chem. 86 (1982) 1822.
13 A.B. Myers, R.A. Mathies, D.J. Tannor and E.J. Heller, J. Chem. Phys., 77 (1982) 3857.
14 L. Tutt, D. Tannor, E.J. Heller and J.I. Zink, Inorg. Chem. 21 (1982) 3859.
15 C.S. Yoo and J.I. Zink, Inorg. Chem. 22 (1983) 2476.
16 L. Tutt, D. Tannor, J. Schindler, E.J. Heller and J.I. Zink, J. Phys. Chem., 87 (1983) 3017.
17 Y.Y. Yang and J.I. Zink, J. Am. Chem. Soc., 106 (1984) 1500.
18 Y.Y. Yang and J.I. Zink, Inorg. Chem., submitted for publication.
19 M.S. Wrighton, G.S. Hammond and H.B. Gray, J. Am. Chem. Soc., 93 (1971), 4336.
20 M.S. Wrighton, H.B. Abrahamson and D.L. Morse, J. Am. Chem. Soc., 98 (1976) 4105.
21 R.M. Dahlgren and J.I. Zink, Inorg. Chem. 16 (1977) 3154.
22 R.M. Dahlgren, Ph.D. Thesis, University of California, Los Angeles, 1978.
23 G. Boxhoorn, A. Oskam, E.P. Gibson, R. Narayanaswamy and A.J. Rest, Inorg. Chem., 20 (1981) 783.

24 A.F. Schreiner, S. Amer, W.M. Duncan, G. Ober, R.M. Dahlgren and J.I. Zink, J. Am. Chem. Soc., 102 (1980) 6871.
25 S.A. Wallin and A.F. Schreiner, Inorg. Chem. 22 (1983) 1964.
26 G. Boxhoorn, D.J. Stufkens, P.J. M. van de Coolwijk and A.M.F. Hezemans, Inorg. Chem., 20 (1981) 2778.
27 M.J. Incorvia and J.I. Zink, Inorg. Chem., 13 (1974) 2489.
28 J.I. Zink, Inorg. Chem., 12 (1973) 1018.
29 J.I. Zink, J. Am. Chem. Soc., 94 (1972) 8039.
30 M. Wrighton, H.B. Gray and G.J. Hammond, Mol. Photochem., 5 (1973) 165.
31 H.G. Van Quickenbourne and A.J. Ceulemans, J. Am. Chem. Soc., 99 (1977) 2208.
32 J.I. Zink, J. Am. Chem. Soc. 96 (1974) 4464.
33 R.A. Brown and G.R. Dobson, Inorg. Chim. Acta, 6 (1972) 65.
34 A.M. English, K.R. Plowman and I.S. Butler, Inorg. Chem., 20 (1981) 2553.
35 L. Dubicki and R.L. Martin, Aust. J. Chem. 22 (1969) 1571-1587.
36 (a) D.S. Martin, R.A. Newman and R.E. Fanwick, Inorg. Chem., 18 (1979) 2511-2520; (b) Ibid., 21 (1982) 3400.
37 F.A. Cotton, D.S. Martin, P.E. Fanwick, T.J. Peters and R. Webb, J. Am. Chem. Soc., 98 (1976) 4681-4682.
38 J.G. Norman, H.J. Kolari, H.B. Gray and W. Trogler, Inorg. Chem., 16 (1977) 987-993.
39 W.C. Trogler, E.J. Solomon, I. Trajberg, C.J. Ballhausen and H.B. Gray, Inorg. Chem. 16 (1977) 828-836.
40 W.C. Trogler and H.B. Gray, Acc. Chem. Res. 11 (1978), 232-239.
41 M.C. Manning and W.C. Trogler, Inorg. Chem., 21 (1982) 2797-2800.
42 H. Yersin, H. Otto, J.I. Zink and G. Gliemann, J. Am. Chem. Soc. 102 (1980) 951-955 and references therein.
43 P.T. Manoharan and H.B. Gray, Inorg. Chem., 5 (1966) 823.
44 L.P. Ziegler and A.C. Albrecht, J. Raman Spectroscopy, 8 (1979) 73.